ISIJ International, Vol. 56 (2016), No. 10, pp. 1874–1883

A Comparison between Ultra-high-strength and Conventional High-strength Fastener Steels: Mechanical Properties at Elevated Temperature and Microstructural Mechanisms

Carin Emmy Ingrid Christersdotter OHLUND,[1,2)]* Mladena LUKOVIC,[3)] Jonathan WEIDOW,[4)] Mattias THUVANDER[4)] and Sven Erik OFFERMAN[2)]

1) Nedschroef Techno Center, Postbus 29, 5700 AA Helmond, The Netherlands. 2) Department of Materials Science and Engineering, Delft University of Technology, Mekelweg 2, 2628 CD, Delft, the Netherlands. 3) Department of Structural Engineering, Delft University of Technology, Stevinweg 1, 2628 CN Delft, The Netherlands. 4) Department of Applied Physics, Chalmers University of Technology, SE-412 96 Gothenburg, Sweden.

(*Received on April 14, 2016; accepted on June 20, 2016*)

A comparison is made between the mechanical properties of the ultra-high-strength steel KNDS4 of fastener grade 14.9 and of conventional, high-strength steels 34Cr4 of fastener grade 12.9 and 33B2 of grade 10.9. The results show that the ratio of the yield strength at elevated temperatures to the yield strength at room temperature is higher for the ultra-high-strength steel than for both conventional high-strength steels, especially at 500°C. Moreover, the results show a trend in which the nano-indentation creep rate is lower as the strength of the steels is higher. The improved mechanical properties of the KNDS4 steel compared to the conventional high-strength steels are related to the smaller size of the alloy carbides in the KNDS4 steel. Furthermore, the effect of an alternative (industrial) heat-treatment on the evolution of the microstructure and hardness of the KNDS4 steel was investigated. Changing the industrial heat treatment can increase the hardness of KNDS4 by about 8%, since more alloy carbides can nucleate and grow. However, the standard industrial heat treatment results in a refinement of the martensite microstructure (grain size), which might be more beneficial for the toughness of the steel. Independent of the heat treatment, the mechanical performance of KNDS4 fasteners at elevated temperature and the low nano-indentation creep rates are two strong indicators that fasteners made from KNDS4 steel might be used at higher service temperatures than traditional high strength fasteners.

KEY WORDS: martensite; alloy carbide; temperature resistance; nano-indentation; strength; microstructure; creep.

1. Introduction

The trend of engine down-sizing has led to smaller engines with higher mechanical and thermal loading of the components inside the engine. High-strength engine fasteners must therefore be able to maintain a high yield strength at elevated temperatures and to withstand creep at elevated temperatures. Martensitic, low- and medium-carbon steels, alloyed with mainly manganese and boron or manganese and chromium, are the work-horse materials for the current high-strength engine fasteners. These fasteners have a tensile strength up to 1 200 MPa and a yield strength of 0.9 times the tensile strength (grade 12.9), according to international fastener standards.[1)] Higher strength fasteners are not yet listed in the fastener standards, because the susceptibility to hydrogen embrittlement increases in case the strength of traditional fastener steels exceeds 1 200 MPa.[2,3)] The fastener standards furthermore state a recommended service temperature of maximum 150°C.[1)] The reason behind the latter restriction is related to the fact that the traditional fastener steels can lose strength and/or experience creep at elevated temperatures.

New fastener steels have already been developed, based on the need for higher strength and improved resistance to hydrogen embrittlement.[4,5)] The improvement in strength at room temperature of these fastener steels is achieved by a tempered martensite matrix and the addition of carbide-forming elements such as titanium, vanadium and molybdenum,[6–11)] that generate precipitation strengthening via formation of alloy carbides. The potential improvements of the mechanical properties of fastener steel at elevated temperatures due to the formation of alloy carbides were not taken into account during the development of novel ultra-high-strength steels for fasteners. However, literature shows that the creep properties of martensitic steel for applications in power plants are improved by the presence of alloy carbides.[12–14)] Moreover, a report has demonstrated the combined improvement of the room temperature and high temperature tensile strengths of martensite due to a fine dispersion of alloy carbides.[15)]

Creep measurements are very time consuming. In this study we aim to obtain more insight into the mechanical properties of ultra-high-strength steels for fasteners at elevated temperatures without performing laborious creep measurements. Instead, we apply the more recently developed technique of nano-indentation.

The aim of the present study is 1) to compare the mechan-

* Corresponding author: E-mail: e.ohlund@nedschroef.nl
DOI: http://dx.doi.org/10.2355/isijinternational.ISIJINT-2016-120

ical properties of the ultra-high-strength steel KNDS4 of fastener grade 14.9 and of conventional high-strength steels 34Cr4 of fastener grade 12.9 and 33B2 of grade 10.9 at room temperature and at elevated temperatures, 2) to characterize the alloy carbides in the steels in order to investigate the underlying microstructural mechanisms that give rise to the different properties of the three fastener steels and 3) to optimize the thermal processing of the ultra-high-strength KNDS4 steel for fasteners. KNDS4 contains the strong carbide-forming elements V, Ti and Mo. These elements form complex alloy carbides during heat treatment and we therefore expect that KNDS4 can have better mechanical properties at elevated temperatures than conventional high-strength steels for fasteners.

2. Experimental

The following three experiments are carried out: 1) mechanical testing of fasteners made of KNDS4, 34Cr4 and 33B2 steel to compare room temperature and elevated temperature mechanical properties, 2) characterization of the alloy carbides to investigate the underlying microstructural mechanisms that give rise to the different properties of the three fastener steels and 3) optimizing the thermal processing of KNDS4 in order to further improve the mechanical properties of the steel. The chemical composition of the investigated steels are shown in **Table 1**. The Fe–C–Mn–Ti steel of an earlier investigation,[16,17] is used as a reference steel for the optimization of the thermal processing of KNDS4 steel.

2.1. Mechanical Testing of KNDS4, 34Cr4 and 33B2 Fasteners

We compare the performance of the different fastener steels at elevated temperature by measuring 1) the yield strength as a function of temperature and 2) the nano-indentation creep rate of the three steels. Traditional creep measurements are time consuming. Therefore, we choose to estimate the relative creep behaviour of the three steels by comparing the tendency for deformation of these steels under constant-load conditions during nano-indentation experiments. We perform these experiments at room temperature, based on literature reports that a large number of metallic materials exhibit indentation creep at temperatures down to room temperature.[18]

We prepare the test specimens from traditionally cold-formed M14 fasteners made from KNDS4, 33B2 and 34Cr4 steel. The fasteners are industrially heat-treated in continuous belt furnaces with oil quenching. The heat-treatment parameters and the room temperature tensile strength and yield strength after heat treatment of the three steels are given in **Table 2**. The longer times for the industrial heat-treatment of KNDS4 are a recommendation from the steel producer. A separate batch of specimens received an additional heat-treatment for 100 hours at 200°C, 300°C, 400°C or 500°C. These are the test temperatures for mechanical property evaluation (see next paragraph). The accuracy of the industrial furnace is ±5°C.

We perform tensile tests on bar-shaped specimens with a diameter of 12 mm and a length of 135 mm, which are machined out of heat-treated fasteners. The specimens have a reduced diameter of 4.00±0.02 mm over a length of 22±2 mm in the middle of the specimen. The radius of curvature of the transition region from the reduced to the full diameter is 30 mm. Tensile testing is performed at room temperature and at elevated temperatures, using a table top MTS 858 system (25 kN) operated in displacement mode. Heating is performed using an induction coil surrounding the test specimen with an ultra-high frequency induction generator TruHeat HF 3005 with a capacity of 6 kW. The temperature of the specimens is measured using three K-type thermocouples, which are separated by approx. 3 mm and which make contact with the specimen by using small springs.[19] The middle thermocouple is used for temperature control. The heating rate is 10°C/s, followed by 5 seconds soaking time at the test temperature, prior to axial loading. Axial loading is performed using a constant strain rate of 0.136 s^{-1} until fracture, following the demand on maximum cross head speed from ISO898-1.[1]

The nano-indentation creep measurements are performed on electro-polished steel specimens using an Agilent G200 nano-indenter equipped with a Berkovich-indenter. The tip is calibrated using a reference specimen of fused silica. We perform 20 indentation experiments on each specimen under constant-load conditions.[20] The maximum load, F_{max}, is 16 mN for all specimens. The load is selected to assure an indentation depth of minimum 150 nm, in order to measure macroscopic behaviour of the material.[21] The indenter is loaded up to F_{max} during 20 seconds. The maximum load is thereafter maintained for 600 seconds, while measuring the indentation depth. After the constant load section is finished the load is decreased to $0.2F_{max}$ and maintained for 20 seconds to investigate thermal drift.

The experiments are evaluated according to the method proposed by Goodall *et al.*[20] Goodall *et al.* propose the parameter P, the tendency of a material to deform under constant-load nano-indentation, for comparing creep behaviour of different materials at a given temperature. The parameter P is defined by:

$$P\left(t^*,\sigma\right)=\Delta h\left(\frac{dh}{dt}\right)_t, \quad \text{..... (1)}$$

where Δh is the distance the indenter has penetrated into the material between the start of the constant-load section and the evaluation time t^*, $(dh/dt)_t$ is the gradient of the depth-time curve at the evaluation time t^* and σ is the applied stress.

During indentation experiments the stresses in the metal, under the indenter, range from high in the vicinity of the

Table 2. Heat treatment parameters of industrial fastener steels (with quenching after the isothermal treatments) and resulting tensile strength and yield strength at room temperature. Error values are given in 95% confidence interval.

Steel	Austenitization	Tempering	R_m (MPa)	Yield strength (MPa)
33B2	890°C, 45 min	460°C, 50–55 min	1 094±12	989±4
34Cr4	890°C, 45 min	460°C, 50–55 min	1 339±10	1 081±6
KNDS4	925°C, 60 min	550°C, 90 min	1 504±16	1 267±17

Table 1. Main elements of the examined steels.

Steel	C	Mn	Si	P	S	Al	Cr	Mo	Ni	Ti	V	B
KNDS4	0.39	0.45	0.05	0.004	0.006	0.033	1.07	1.09	0.60	0.042	0.085	–
34Cr4	0.36	0.85	0.10	0.006	0.007	0.036	1.09	0.050	0.05	0.001	0.003	–
33B2	0.32	0.72	0.09	0.010	0.010	0.031	0.23	0.008	0.04	0.051	0.004	0.002
Fe–C–Mn–Ti	0.39	0.87	0.004	0.001	0.001	0.005	0.00	–	–	0.042	0.002	–

indenter tip, to low values far from the indenter tip. Studies have shown that dislocation glide is the main mechanism by which nano-indentation creep takes place, due to the high stresses near the indenter tip. However, nano-indentation creep in materials with small grain sizes may as well be dominated by Coble (diffusional flow) creep.[18] Since the steels in our investigation have grain sizes that are smaller than 0.4 μm, we expect that diffusional creep may be involved.

Goodall *et al.*[20] suggest that different materials should be compared at the same time, t^*, and load, F_{max}, during indentation experiments. We therefore evaluate the parameter P for the three steels at $t^* = 570$ *s*. However, since the three investigated steels have different hardness, the evaluation at $t^* = 570$ *s* will result in different indent depths. This will result in different contact pressures between the indenter and the steels, since all experiments are done at similar load. High contact pressures are expected to generate a higher degree of dislocation glide plasticity. We therefore also evaluate the parameter P for the three steels at the same depth; *i.e.* at the same σ but different t^*. Evaluation at similar depth allows us to compare the nano-indentation creep of the three steels at the same contact pressure.[22] The evaluation at a similar depth is done at $\Delta h = 300 \pm 20$ *nm*, since this indent depth is reached during the constant hold period at a point where the depth-time curve has stabilized to a linear trend for all three steels.

2.2. Characterization of Alloy Carbides in KNDS4 and 34Cr4

The volume fractions of alloy carbides that are potentially present in the alloys are calculated with ThermoCalc software using the database TCFE06. The alloy carbides in the steels are experimentally characterized by Atom Probe Tomography (APT). The specimen preparation method for APT is described elsewhere.[16] The ATP analyses are performed using laser pulsing. The pulse frequency is set to 200 kHz, the laser energy to 0.25 nJ, the specimen temperature to 50 K and the evaporation rate to 0.5%. The reconstruction and data evaluation is performed using the IVAS 3.6.1 software. The quantitative analysis is based on the isotope distribution of different ions of the relevant atoms.[23] The APT measurements are only performed for the KNDS4 and 34Cr4 steels, since steel 33B2 has a low fraction of alloy carbides (see **Fig. 4**) and because the tensile-to-yield strength ratio of 33B2 is slightly lower than 34Cr4 (see section 3.1 and **Fig. 2**).

2.3. Optimization of the Thermal Processing of KNDS4

We explore if it is possible to improve the mechanical properties of KNDS4 steel by austenitizing the steel at 1 350°C instead of 940°C, which is the maximum capacity of the current industrial heat treatment equipment. The idea behind the alternative heat-treatments is to dissolve more alloying elements at higher temperatures in order to obtain a high density of small alloy carbides and cementite during subsequent tempering. The soaking time at 1 350°C is chosen to 30 minutes in order to compare the results to our earlier studies.[16,17] We note that ThermoCalc simulations show that a small volume fraction of $Ti_4C_2S_2$ phase can form in the temperature range of 1 070°C to 1 456°C. It may therefore not be possible to assure that all Ti-atoms are in solid solution. The KNDS4 steel that is quenched from 1 350°C is from here on called KNDS4_1350 and the KNDS4 steel that is quenched from 940°C is called KNDS4_940. The austenitization treatment is followed by quenching to room temperature using He-gas, which resulted in a cooling rate of approx. 175–180°C/s from the start of quench to the martensite start (M_s) temperature and a cooling rate of approx. 45˚C/s below the M_s-temperature. All specimens are subsequently isothermally tempered at 550°C for 5, 10, 30 or 60 minutes in order to study the evolution of the microstructure and the hardness with time during tempering. The heating time to the isothermal tempering temperature is 138 s. The tempering temperature of 550°C is chosen because it correlates with industrial heat-treatment of KNDS4 steel and in order to stay in line with our earlier investigations.[16,17]

The heat-treatments are performed on steel specimens that are machined to a cylindrical shape with a diameter of 4 mm and a length of 10 mm. The specimens are heat-treated in a Bähr 805 A/D dilatometer (Bähr-Thermoanayse GmbH, Hüllhorst, Germany).

Optical microscopy and scanning electron microscopy (SEM) (JEOL JSM-6500F with a field emission gun) is performed on nital-etched (5%) surfaces. Electron backscatter diffraction EBSD (using the SEM with a Nordlys detector) is performed on electro-polished surfaces, conducted in a solution of 8% perchloric, 10% butylcellosolve, 60% ethanol and 22% water. The EBSD data is acquired and post-processed with Channel 5 software. The beam diameter during EBSD mapping is approx. 16 nm, resulting in a spot dimension of 16 nm × 35 nm. This spot dimension is combined with a step size of 100 nm. Conventional micro-Vickers hardness is measured at 20 locations using a load of 500 g.

3. Results and Discussion

3.1. Mechanical Testing

3.1.1. Yield Strength

Figure 1 shows examples of stress-strain curves measured at room temperature and at 500°C for the three investigated steels. The yield strength reduces with increasing temperature, for each of the three steels. Figure 2 shows the ratio of the yield strength at elevated temperature to the yield strength at room temperature of industrially heat treated 33B2, 34Cr4 and KNDS4 fastener steels as a function of test temperature after 5 seconds of soaking time and

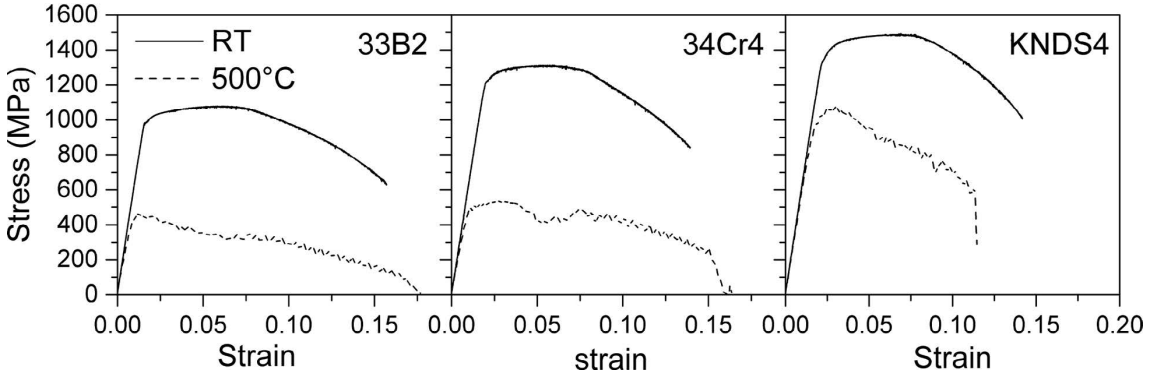

Fig. 1. Examples of stress-strain curves measured at room temperature and at 500°C for 33B2. 34Cr4 and KNDS4.

after 100 hours of soaking time. The yield strength ratio at 500°C is $\sigma/\sigma_0 \approx 0.65 \pm 0.06$ for the KNDS4 steel, which is much higher than the yield strength ratio at 500°C of $\sigma/\sigma_0 \approx 0.40 \pm 0.04$ for the 34Cr4 and 33B2 steels (for which the yield strength ratios are similar). Furthermore, the yield strength ratio of KNDS4 at 500°C is the same after 100 hours of soaking time as after 5 seconds of soaking time. The improved properties of the KNDS4 steel are believed to be a result of secondary alloy carbides, which form during the tempering of KNDS4. This is discussed in later sections. **Table 3** shows the data list, used to create Fig. 2.

3.1.2. Nano-indentation Creep Rate

Figure 3 shows (a) the tendency of the three steels to deform under constant load nano-indentation, P (Eq. (1)), as evaluated both at $t^* = 570$ s and at indent depth 300 ± 20 nm and (b) examples of the load displacement curves up to the constant load for the three steels. Figure 3(a) shows that the KNDS4 steel has a lower tendency to deform than the 34Cr4 and 33B2 steels, which have similar values of P. Figure 3(a) furthermore shows that at similar depth, $\Delta h = 300 \pm 20$ nm the tendency to deform decreases with increasing tensile strength of the three steels; KNDS4 steel shows the smallest tendency to deform and steel 33B2 shows the highest tendency to deform.

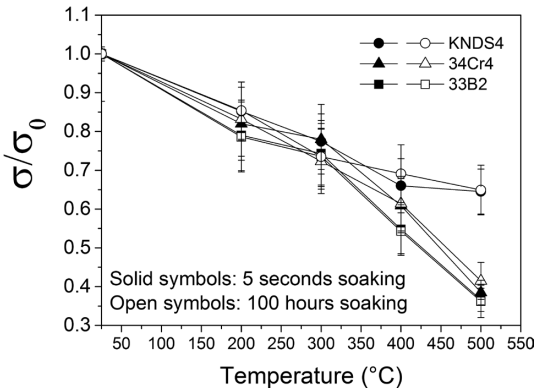

Fig. 2. Yield strength ratio, σ_0 is the room-temperature yield strength, of industrially heat treated 33B2, 34Cr4 and KNDS4 steel as a function of test temperature after 5 seconds and 100 hours soaking time. Error bars represent 95% confidence interval.

Table 3. Yield strength (MPa) at elevated temperatures. Error values are given in 95% confidence interval.

Steel	200°C	300°C	400°C	500°C
33B2	782 ± 8	735 ± 11	541 ± 34	363 ± 12
33B2 (100 hr soaking)	777 ± 18	728 ± 4	537 ± 14	359 ± 13
34Cr4	886 ± 22	843 ± 32	658 ± 46	416 ± 23
34Cr4 (100 hr soaking)	889 ± 6	781 ± 7	663 ± 22	448 ± 9
KNDS4	1 053 ± 8	957 ± 13	816 ± 20	798 ± 9
KNDS4 (100 hr soaking)	1 056 ± 2	909 ± 18	855 ± 22	802 ± 15

At similar indentation depth the contact stress between the indenter and the steel samples is similar, since the load is similar. This contact stress is the driving force for nano-indentation creep. Studies have shown that nano-indentation creep is dominated by the mechanism of dislocation movements and that diffusional creep could become significant at grain sizes below 0.4 μm.[18] Studies[24] has showed that higher carbon content in steel leads to a slight reduction of the martensite grain size. The industrial heat treatment of KNDS4 furthermore results in grain refinement due to presence of undissolved Ti-carbides (see section 3.3). KNDS4 is thus expected to have a smaller martensite grain size than 34Cr4 and 33B2 steel and should therefore have a higher contribution of diffusion creep to the nano-indentation creep, as compared to 34Cr4 and 33B2. Figure 3(a) consequently indicates that the microstructure of KNDS4 generates the highest resistance to dislocation movements (glide plasticity) of the three examined steels. The better performance of the KNDS4 steel is believed to be a result of a higher density of small and stable alloy carbides that prevent dislocation movements in the KNDS4 steel. Comparing the three steels, KNDS4 is expected to have the lowest dislocation density and 34Cr4 the highest. Litterature[25,26] reports that a higher carbon concentration results in a higher dislocation density of as-quenched martensite. Quenched KNDS4 should have approximately 3% and 6% higher dislocation density, than 34Cr4 and 33B2 respectively. However, the subsequent tempering will lead to a marked reduction in dislocation density that is controlled by the tempering temperature. This reduction in dislocation density is expected to be in the range 30% for tempering at 460°C and 50% for tempering at 550°C.[27] The nucleation of alloy carbides in KNDS4 and 34Cr4 will prevent some dislocation recovery, but only a few %, since the tempering is continued for 60 minutes.[17] We emphasize that the parameter P does not represent fundamental creep characteristics, but is only used to compare the behavior of the three fastener materials to each other. Traditional axial creep testing is required in a subsequent study to fully establish the creep performance of the KNDS4 steel.

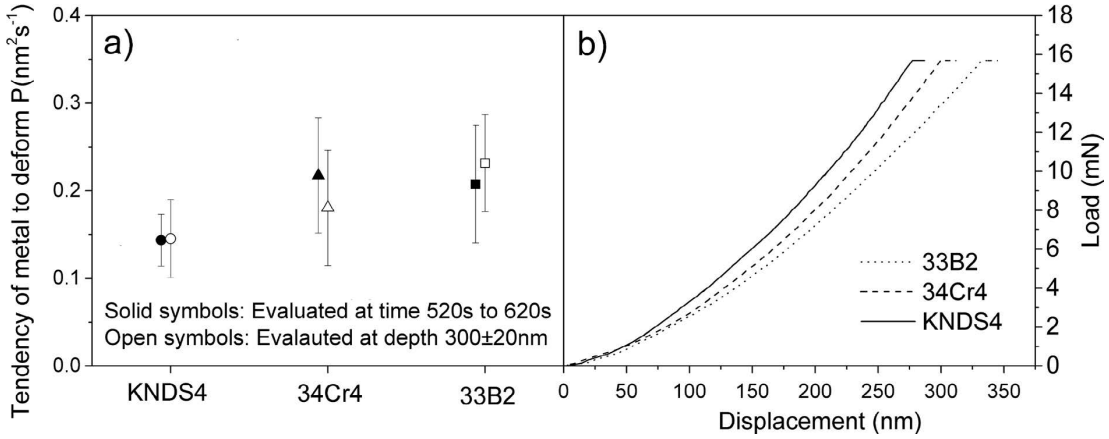

Fig. 3. Nano-indentation measurements showing (a) the tendency of the three steels to deform under constant load nano-indentation, the parameter P (Eq. (1)) evaluated at the end of the constant load period (solid symbols) and at indent depth 300 nm (open symbols) and (b) examples of lead-displacement curves up to the constant load. Error bars represent 95% confidence interval.

3.2. Characterization of the Alloy Carbides

3.2.1. ThermoCalc Study

Figure 4 shows the mole fraction of stable alloy carbide phases in the KNDS4, 34Cr4 and 33B2 steels, as a function of temperature, as calculated using ThermoCalc. Phases with a mole fraction less than 0.0005 are excluded from the figure.

The fractions of stable alloy carbide phases are significantly higher in the KNDS4 and 34Cr4 steel than in the 33B3 steel, at the tempering temperature during the industrial heat treatment. The equilibrium alloy carbides in KNDS4 steel at 560°C are M_7C_3, $M_{23}C_6$, TiC and MC-type. The M_7C_3-phase has the highest mole fraction. The main equilibrium alloy carbide in steel 34Cr4 is the M_7C_3-phase. The main alloy carbide type of 33B2 steel is of FCC-type consisting mainly of C, Ti and Cr.

The higher mole fractions of alloy carbides in KNDS4 and 34Cr4 can lead to increased precipitation strengthening if the mole fraction is divided into a fine distribution of small alloy carbides. Small precipitates can reduce the mobility of dislocations at both room temperature and elevated temperature. This can increase the yield strength ratio at elevated temperatures and reduce creep rates of KNDS4 and 34Cr4 steels.

At the austenitization temperature of the industrial heat treatment of KNDS4 steel the equilibrium mole fraction of TiC is 0.0015, which means that the majority of the Ti-atoms does not dissolve in the austenite. Therefore, we expect that the formation of the TiC is limited during industrial tempering of KNDS4 steel. The pre-existing, primary TiC-precipitates are expected to be course compared to the secondary TiC-precipitates that can form during tempering.[28)]

3.2.2. APT Study of KNDS4 and 34Cr4

Atom probe tomography measurements are performed on the KNDS4 and 34Cr4 steels. We exclude steel 33B2 from the APT study, because the ThermoCalc calculations show that the fraction of alloy carbide precipitates is very low in steel 33B2 and because the tensile-to-yield strength ratio of 33B2 is slightly lower than 34Cr4. **Table 4** shows the equilibrium compositions (at%) of the stable phases in the KNDS4 and 34Cr4 steels as calculated with ThermoCalc. Furthermore, Table 4 shows the composition of the

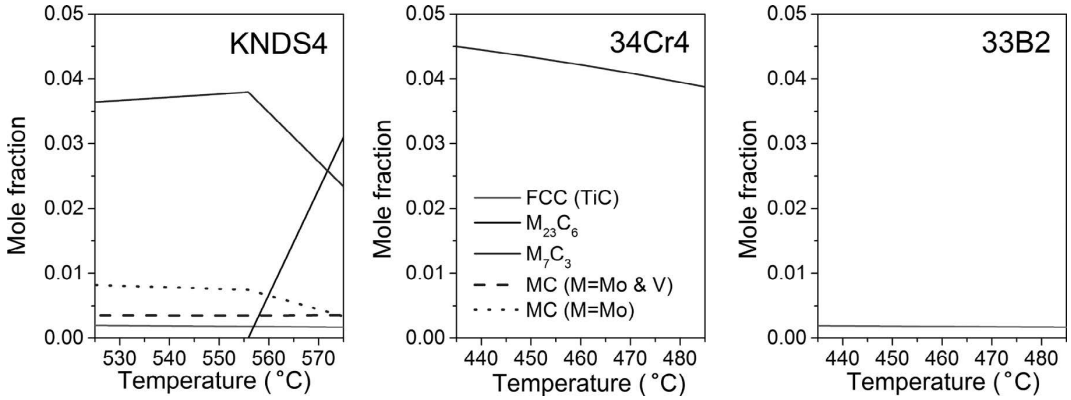

Fig. 4. Fractions of stable alloy carbide phases in KNDS4, 34Cr4 and 33B2 steel as a function of temperature, in the temperature range around the tempering temperature.

Table 4. ThermoCalc equilibrium concentrations of C, Mn, Cr, Mo, V and Ti in the matrix and in stable phases of KNDS4 and 34Cr4 at the tempering temperature and the APT measurements [at%]. Error values are given in standard deviation. The APT measurement of the matrix is given without error since only one sample was measured.

	C	Mn	Cr	Mo	V	Ti
KNDS4						
Matrix	0.007	0.23	0.14	0.03	0.00	0.00
Measured matrix (APT)	0.34	0.52	0.97	0.55	0.07	0.00
Cementite	25.0	4.6	9.2	0.3		
M_7C_3	30.0	6.0	25.4	3.8	0.1	
$M_{23}C_6$	36.3	0.8	33.6	8.4	0.03	
MC_ETA	50.0			25.8	24.2	
FCC_TiC	49.9	0.1	18.7	0.6	1.2	27.0
MC_SHP	50.0			50.0		
Measured large carbides (ATP)	(25)	1.9±0.4	2.6±0.4	1.7±0.1		
Measured small carbides (ATP)	(30)	4.7±2.2	6.0±1.0	5.1±0.7	0.5±2	0.0
34Cr4						
Matrix	0.001	0.19	0.05	0.00	0.00	
Measured matrix (APT)	0.20	0.79	1.07	0.09	0.00	
Cementite	25.0	8.3	7.9	0.1		
M_7C_3	30.0	12.7	23.4	0.5		
Measured large carbides (ATP)	(25)	0.9±0.1	1.5±0.2	0.06±0.02	0.004±0.002	
Measured small carbides (ATP)	(30)	5.4±2.3	8.9±3.3	0.17±0.12	0.04±0.02	

matrix and alloy carbides as measured by APT. The APT measurements show that the concentrations of the alloy elements in the matrix of KNDS4 and 34Cr4 steels after the heat-treatment are similar to the overall composition of the steel, as given in Table 1. Therefore, we conclude that the redistribution of alloying elements into both cementite and alloy carbides does not significantly affect the average composition of the matrix during tempering up to 60 minutes. After 60 minutes of tempering the martensite matrix is still supersaturated with alloying elements. Further growth, and possible nucleation, of alloy carbides is therefore likely to take place during prolonged tempering of both steels (although we did not investigate this). Ti-atoms were not detected with APT in the KNDS4 specimen. This could be the result of the spatial distribution of the stable, primary TiC carbides (which were not present in the investigated volume), and the low concentration of Ti-atoms in solid solution that is below the resolution of the APT detection level (affected by the detection efficiency of 37%). ThermoCalc simulations show that at 940°C the mole fraction of stable TiC-precipitates is 0.002 and that only $9 \cdot 10^{-6}$ wt% Ti is in solid solution.

Figure 5 shows APT images of industrially heat treated KNDS4 (a) and 34Cr4 (b) steel where carbon atoms are shown as red dots, cementite is shown as blue iso-concentration-surfaces and alloy carbides are shown as green iso-concentration-surfaces. The carbides (cementite and alloy carbides) are distinguished from the surrounding matrix by the carbon concentration. The APT measurements of the carbon concentration in the matrix are 0.20 at% and 0.34 at% in KNDS4 and 34Cr4, respectively, whereas all measured carbides contain a carbon concentration that exceeds 10 at% C. The cementite and alloy carbides are thereafter separated by comparing the Cr, Mn and Mo concentrations, after adjustment of the atom count.

The atomic concentrations, as measured by APT, cannot be directly compared to the compositions as calculated by ThermoCalc, since the overall detection efficiency of the APT instrument is limited and due to that some matrix atoms will be included inside the voxels which encapsulate the surface of the carbides. Small carbides are more affected by included matrix in the surface voxels. Furthermore, carbon atoms might not be detected due to surface migration,[29] and the measured carbon concentration might be too low due to detector pile-up.[23]

Figure 4 shows that the stable carbides of 34Cr4 steel at the industrial tempering temperature are cementite and M_7C_3. The main difference between these carbides is the concentration of Mn and Cr. The APT measurements showed that the smaller carbides are significantly more enriched in Cr and Mn than the large carbides. The APT measurement of the smaller carbides are 2.5±0.8 at% Mn and 3.9±1.3 at% Cr, whereas the APT measurement of the larger carbides are 1.0±0.2 at% Mn and 1.6±0.4 at% Cr, respectively. This indicates that the smaller carbides are M_7C_3 and that the larger carbides are cementite. We note that matrix atoms are included in the voxels of these carbides. Including matrix atoms will act to "dilute" the concentration of Mn and Cr. This effect should be more pronounced for the M_7C_3 carbides since these are smaller. In order to correct our APT measurements of the small carbides, we therefore remove matrix atoms from the atom count of the carbides until we reach the expected carbon concentration of both carbides (25 at% and 30 at% for cementite and M_7C_3 respectively). The corrected values are presented in Table 4.

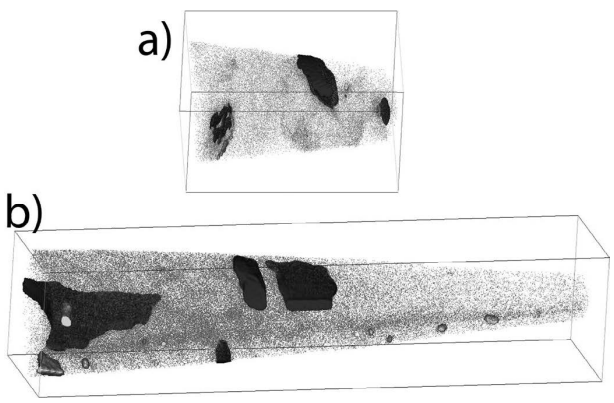

Fig. 5. APT images of as-quenched steels where carbon atoms are shown as red dots, cementite is shown as blue iso-surfaces and alloy carbides are shown as green iso-surfaces: (a) KNDS4, length 176 nm and (b) 34Cr4, length 469 nm.

Figure 4 shows that the stable carbides of KNDS4 at the industrial tempering temperature are cementite, M_7C_3, $M_{23}C_6$, and three types of MC carbides. The APT measurements of the carbides in the KNDS4 steel did not show any clear and significant difference in composition comparing the small and the large carbides. The APT measurements did however show that none of the measured carbides are of MC type. The FCC (TiC) carbide can be excluded since none of the measured carbides contain Ti. The MC (ETA) carbide can be excluded since none of the measured carbides contained Mo and V in 1:1 relationship and the MC (SHP) carbide can be excluded since none of the measured carbides contain high levels of Mo, combined with no or low levels of the other alloy elements. The carbides measured by APT in KNDS4 are therefore expected to be $M_{23}C_6$, M_7C_3 or cementite. We note that when matrix atoms are included in the voxels of any of the carbides in KNDS4 (the voxels at the surface of the carbides), this will act to "dilute" the concentration of Mn, Cr and V in all of the three possible carbides ($M_{23}C_6$, M_7C_3 and cementite). In order to correct our APT measurements for the carbides we therefore remove matrix atoms from the atom count of the carbides. We note that when the composition is corrected, the content of Mn increases above 0.8 at% in all carbides. None of the carbides is therefore expected to be of $M_{23}C_6$ type. When the carbides are compared at 25 and 30 at% C, the average alloy composition of element Mn, Cr and Mo in the carbides starts to indicate that the small and the large carbides are of different types. The corrected values are given in Table 4. The higher alloy content of the smaller carbides indicates that these are of M_7C_3 type, whereas the larger carbides are cementite. In order to confirm the distinction between alloy carbide and cementite a characterization of the crystal structure would be necessary, which is not possible in APT.

The average number of atoms measured in the alloy carbides are 330±290 atoms in KNDS4 and 3 270±2 500 atoms (95% confidence interval) in 34Cr4. We calculate the average sizes of the alloy carbides by assuming spherical shape. M_7C_3 carbides have an orthorhombic crystal structure with lattice parameters $a=0.4526$ nm, $b=0.7010$ nm and $c=1.2142$ nm and 40 atoms per unit cell[30]). We calculate that the average alloy carbide diameter is 1.8 nm in KNDS4 steel and 3.9 nm in 34Cr4.

The strengthening effect of the alloy carbides, $\Delta\sigma_P$ is thereafter estimated according to the Orowan-Ashby equation:[31]

$$\Delta\sigma_P = \left(\frac{0.538Gbf^{1/2}}{d}\right)\cdot\ln\left(\frac{d}{2b}\right), \quad \text{..... (2)}$$

where d is the average precipitate diameter, G is the shear modulus of the matrix (calculated to be 80.4 GPa by a linear interpolation between the systems of Fe and Fe-1C at a concentration of 0.4 wt%C[17]), b is the length of the Burgers vector (0.248 nm[11]) and f is the volume fraction of

precipitates. We use the ThermoCalc simulation values of the mole fractions at the respective tempering temperature of KNDS4 and 34Cr4 as input for *f*. We thereafter convert the strength to hardness HV using $HV = \sigma_P/3$.[24]

The strengthening effect of the alloy carbides in KNDS4 contributes to 492 HV hardness and the alloy carbides in 34Cr4 contribute 387 HV hardness. We note that this calculation represent the strengthening effect of the equilibrium volume fraction of alloy carbides in the two steels, and therefore is an over-estimation. The higher strengthening effect of the carbides in the KNDS4 compared to the 34Cr4 steel (due to the smaller size) does, however, indicate that the pinning effect of the alloy carbides is higher in KNDS4. The better yield strength ratio of KNDS4 at elevated temperatures is therefore considered to be a result of the smaller alloy carbide precipitate size in KNDS4, as compared to 34Cr4. The small alloy carbide precipitates of KNDS4 will hinder the dislocation motion, which in turn reduces the nano-indentation creep rate of KNDS4.

3.3. Optimizing the Thermal Processing of KNDS4

We compare the microstructure and hardness evolution during tempering of KNDS4 after different austenitization temperatures with the results of earlier investigations that we performed on a model alloy of Fe–C–Mn–Ti steel with similar concentrations of carbon and titanium.[16,17] Studies have shown that the toughness of martensitic structures can be improved by refinement of the martensite (former austenite grain size, packet size and block size[32,33]). It is therefore of importance to avoid coarsening of the microstructure during heat treatment.

3.3.1. Former Austenite Grain Size and Cementite Size

The former austenite grains are measured using the linear intercept method on nital etched specimens. The former austenite grain size of KNDS4_1350 is 750 ± 179 μm, whereas the former austenite grain size of KNDS4_940 is 8 ± 1.5 μm (95% confidence interval). This difference in austenite grain size is directly related to the austenitization temperature since grain growth rate increases with increasing temperature. Moreover, stable TiC and MnS phases hinder the mobility of the austenite grain boundaries during austenitization treatment at 940°C (calculated using ThermoCalc). These phases are not present at 1 350°C, which allow the austenite grains to grow more rapidly in KNDS4_1350.

Figure 6 shows SEM images of (a) KNDS4_1350, (b) KNDS4_940 and (c) Fe–C–Mn–Ti steel at low magnification in the as-quenched state and (d) the average radius of the cementite particles of the three steels as a function of tempering time. The auto-tempered regions in the SEM images (Figs. 6(a)–6(c)) appear as white regions due to the small iron carbides. We note from the SEM images that the degree of auto-tempering is higher in the KNDS4 steels than in Fe–C–Mn–Ti steel. The area fraction of auto-tempered regions is estimated to 80–90% in the two KNDS4 steels, where KNDS4_1350 appears to have slightly more auto-tempering than KNDS4_940, and 40–50% in Fe–C–Mn–Ti steel. The study of individual cementite particle sizes was performed at higher magnification SEM images, which are presented in **Fig. 7**.

The average cementite radius, *R*, is calculated according to:

$$R = \sqrt{\left(\frac{w}{2}\right)\left(\frac{l}{2}\right)}, \quad \text{..... (3)}$$

where *w* and *l* are the average width and length of the cementite particles in the SEM images. The cementite particles grow rapidly during the first 5–10 minutes of annealing. Thereafter, their size stabilizes.

3.3.2. Martensite Block Size and Width of the Block Boundaries

We define the martensite block boundaries as boundaries between two neighboring pixels with a misorientation that exceeds 10°.[34] The average block size is measured from Inverse Pole Figure maps of the martensite. The average martensite block size after quenching is 4.1 μm^2 in KNDS4_1350 and 2.4 μm^2 in KNDS4_940. The spread in grain size is large in both KNDS4 steels. The area of the largest and the smallest grain in KNDS_1350 is 30.0 μm^2 and 0.1 μm^2, respectively. The area of the largest and smallest grain in KNDS4_940 is 19.6 μm^2 and 0.1 μm^2, respectively. We observe that no block coarsening takes place during tempering at 550°C.

In our earlier studies we showed that the regions adjacent to block boundaries in martensite cannot be indexed by EBSD, because these regions contain high dislocation densities.[16,21] The Kikuchi patterns that are obtained dur-

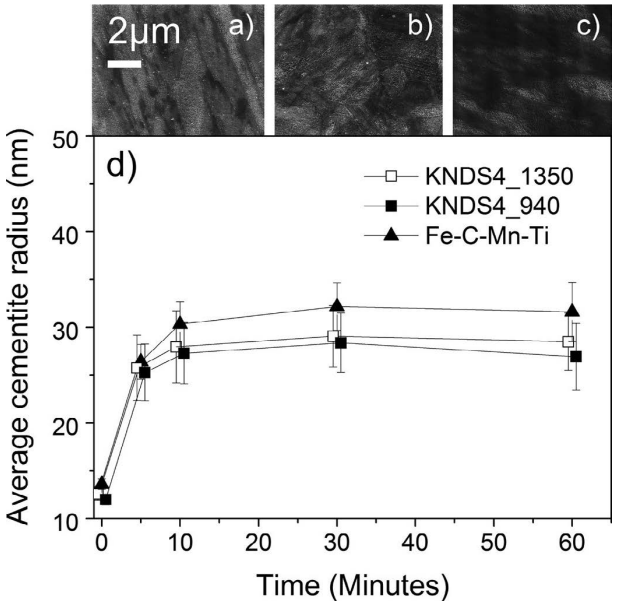

Fig. 6. SEM images of the as-quenched microstructure in a) KNDS4_1350, b) KNDS4_940 and c) Fe–C–Mn–Ti steel and d) the average radius of the cementite particles of the three steels as a function of tempering time at 550°C. Error bars represent 95% confidence interval.

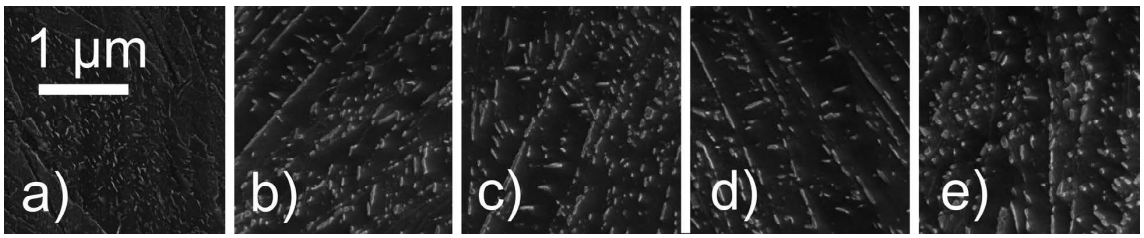

Fig. 7. SEM images of the cementite particles in KNDS4_1350 in a) the as-quenched state and b) after 5 minutes, c) after 10 minutes, d) after 30 minutes and e) after 60 minutes of tempering at 550°C.

ing EBSD measurements are typically degraded by surface roughness, grain boundaries, dislocations or precipitates, which induce strain in the lattice.[35] As stated above, the EBSD results show that block coarsening does not takes place. Therefore, the relative changes in the number of non-indexed points during tempering are a result of changes in the strain level of the steel, *e.g.* via recovery of dislocations and nucleation of precipitates. Recovery leads to a reduction in non-indexed points whereas nucleation of precipitates leads to an increase in non-indexed points since the precipitates are too small to be indexed (the beam spot size will cover both matrix and precipitate) and induce strains in the surrounding lattice. Small carbides will furthermore prevent recovery (by pinning of dislocations). We use the width of the non-indexed regions of the martensite block boundaries to study the evolution of strain in the martensite during tempering.

Figure 8 shows the average width of the non-indexed martensite block boundaries in the KNDS4_1350, KNDS4_940 and Fe–C–Mn–Ti steels, as a function of tempering time at 550°C. In the as-quenched state, the width of the non-indexed block boundaries in the two KNDS4 steels is similar, and a little lower than the width of the non-indexed block boundaries in the Fe–C–Mn–Ti steel. During the first 5 minutes of tempering the width of the non-indexed regions decreases at a high rate in KNDS4_940 and Fe–C–Mn–Ti steel and with a slightly lower rate in KNDS4_1350. The rapid decrease of the non-indexed boundary width in Fe–C–Mn–Ti steel during the first 5 minutes of tempering was shown to be a result of recovery in the martensite in.[16,17]

During tempering from 5 to 10 minutes the width of the non-indexed boundary regions continue to decrease in Fe–C–Mn–Ti, whereas KNDS4_1350 shows a significant increase in the non-indexed boundary width. The increase in the non-indexed boundary width of KNDS4_1350 is a result of rapid nucleation and growth of precipitates. The earlier studies of Fe–C–Mn–Ti steel indicate that TiC-precipitate nucleation and growth takes place between 5 and 10 minutes. The increase in non-indexed points at the block boundaries of KNDS4_1350 steel therefore indicates that a higher density of precipitates nucleates and grows in KNDS4_1350, as compared to Fe–C–Mn–Ti steel.

During tempering from 10 minutes to 30 minutes, the width of the non-indexed boundaries decreases slightly in KNDS4_1350 and Fe–C–Mn–Ti. The slight decrease indicates that recovery takes place in parallel with nucleation and growth of alloy carbides. During tempering from 30 minutes to 60 minutes the width of the non-indexed boundaries in KNDS4_1350 continues to increase again whereas the width of the non-indexed block boundaries continues to decrease in Fe–C–Mn–Ti. The increase observed for KNDS4_1350 indicates that the alloy carbide precipitates in KNDS4_1350 have grown into a size which induces strain in the lattice and distorts the Kikuchi pattern enough to prevent indexing. Since no increase of the width of the non-indexed block boundaries is observed in Fe–C–Mn–Ti, this suggests that the alloy carbides in Fe–C–Mn–Ti are of smaller size and possibly have a lower number density.

Both Fe–C–Mn–Ti and KNDS4_940 show a decreasing width of non-indexed boundaries from 5 minutes of tempering to 60 minutes of tempering. The overall decrease of non-indexed block boundary width in KNDS4_940, from 5 minutes to 60 minutes, suggests that the density of alloy carbides that nucleate and grow during tempering is lower in KNDS4_940 than in KNDS4_1350.

3.3.3. Hardness Evolution with Tempering Time

Figure 9 shows the hardness of KNDS4_1350, KNDS4_940 and Fe–C–Mn–Ti steel as a function of time during tempering at 550°C.

KNDS4_1350 is harder than KNDS4_940, at all tempering times. The hardness difference is 29 HV in the as-quenched state and during the first 10 minutes of tempering and thereafter increases to 37 HV after 60 minutes of tempering. This hardness difference can be caused by (i) different dislocation density, (ii) different concentrations of elements in solid solution, (iii) differences in grain boundary strengthening and/or (iv) different densities of small precipitates. We investigate the root cause to the hardness difference between KNDS4_1350 and KNDS4_940 in the as-quenched state via a review of (i) to (iv).

The EBSD studies showed that the width of the non-indexed block boundary regions of the two KNDS4 steels is similar in the as-quenched state (Fig. 8). We therefore expect that the dislocation density is similar in the two steels. We calculate the difference in the strengthening effect of elements in solid solution of KNDS4_1350 and KNDS4_940 in the as-quenched state according to:[36]

$$\Delta\sigma_{ss} = \sum_i K_i c_i, \quad \text{..... (4)}$$

where K_i is a constant for alloy element i, and c_i is the concentration of element i in weight percent. We assume that all elements that are in solid solution during the austenitization treatment remain in solid solution in the as quenched state. The calculations can therefore lead to differences only for the elements that are present in stable phases at the respective austenitization temperature, since both KNDS4 steels have the same overall composition. ThermoCalc simulations show that TiC-phase and MnS-phase are stable at 940°C and that $Ti_4C_2S_2$ is stable at 1 350°C. The concentration of Ti in solid solution of the austenite is $9{\cdot}10^{-6}$ wt% at 940°C

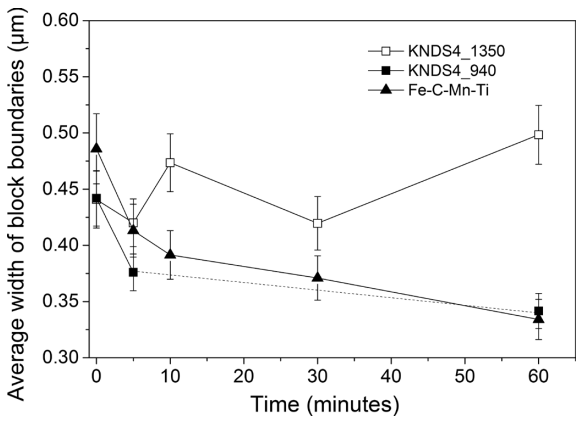

Fig. 8. Width of non-indexed martensite block boundaries in KNDS4_1350, KNDS4_940 and Fe–C–Mn–Ti steel[20] as a function of tempering time at 550°C. Error bars represent 95% confidence interval.

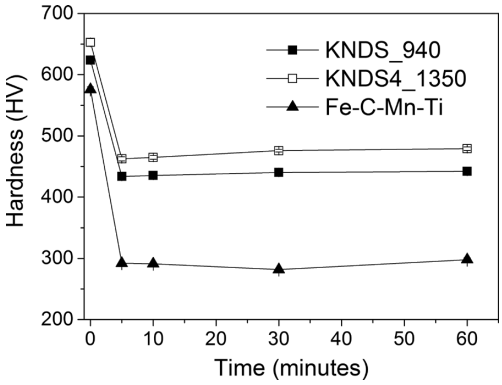

Fig. 9. MicroVickers hardness of KNDS4_1350, KNDS4_940 and Fe–C–Mn–Ti steel, as a function of time during tempering at 550°C. Error bars representing 95% confidence interval are hidden by the symbols.

and 0.03 wt% at 1 350°C and the concentration of Mn in solid solution of the austenite at 940°C is 0.0044 wt%. ThermoCalc furthermore shows that the concentration of S is similar at 940°C and at 1 350°C since S redistributes to MnS at 940°C and to $Ti_4C_2S_2$ at 1 350°C. The calculation is therefore performed only for the elements Ti and Mn. We use K_{Mn}=35 MPa%$^{-1}$ [25] and K_{Ti}=1 680 MPa%$^{-1}$.[17] The calculated hardness difference of KNDS4_1350 and KNDS4_940, due to Mn and Ti is 22 HV, in which KNDS4_1350 is the harder microstructure.

We calculate the strength contribution of the block size of the martensite, σ_{gb}, to the overall strength of KNDS4_1350 and KNDS4_940 using the Hall-Petch equation:[37]

$$\sigma_{gb} = k_{gb} D^{-1/2}, \quad \text{..... (5)}$$

where k_{gb} is the Hall-Petch factor and D the average diameter of the martensite blocks. We use the average block diameter as measured by EBSD.

We use k_{gb} = 17.4 $MPa\ mm^{1/2}$ according to.[11] The strengthening effect of the martensite block is 139 HV in KNDS4_940 and 121 HV in KNDS4_1350.

Taking (i), (ii) and (iii) into account, we expect that precipitates generate a hardness increase of 24.4 HV in KNDS4_1350, in order for our calculations to correlate with the measured hardness difference of 29 HV between KNDS4_1350 and KNDS4_940 in the as-quenched state. There are several precipitate types which can generate precipitation strengthening in KNDS4_1350: M_7C_3 alloy carbides which form during quenching, $Ti_4C_2S_2$ which can form during the austenitization and possibly small iron carbides from auto-tempering.

According to Eq. (2), the smallest precipitate size (diameter) that can generate precipitation strengthening is 0.5 nm. The lattice parameters for M_7C_3 alloy carbides (see section 3.2) show that approx. 7 atoms are needed to form an M_7C_3 precipitate of diameter 0.5 nm. Nucleation of alloy carbides of the type M_7C_3 can therefore rapidly generate precipitation strengthening of the steel. In order to generate 24.4 HV, these small precipitates do however require a volume fraction close to 0.18 and we therefore consider M_7C_3 precipitates which form during quenching an unlikely root cause to the measured hardness difference. ThermoCalc shows that $Ti_4C_2S_2$ is stable in austenite at temperatures higher than 1 070°C. It is therefore possible that $Ti_4C_2S_2$ nucleates as small precipitates during austenitization of KNDS4_1350. The equilibrium volume fraction of $Ti_4C_2S_2$ in KNDS4_1350 is $3.77 \cdot 10^{-4}$ at 1 350°C. This volume fraction of precipitates of size 0.62 nm can generate a hardness increase of 25 HV.

The slight difference in auto-tempering of the two KNDS4 steels after quenching can also generate a hardness difference. Using the average iron-carbide precipitate size and comparing 80% (KNDS4_940) and 90% (KNDS4_1350) auto-tempering, a hardness difference of 12.5 HV can be generated. We therefore conclude that the hardness difference of 24.4 HV can be generated by a combination of different precipitate types in KNDS4_1350.

The increase of the hardness difference between KNDS4_1350 and KNDS4_940, from 29 HV in the as-quenched state, to 35 HV after 30 minutes of tempering confirms the EBSD result that a higher number density of precipitates nucleate and grow in KNDS4_1350 than in KNDS4_940, since no other hardening mechanism leads to increased strengthening in these two steels during tempering (no grain refinement is observed by EBSD, the number of dislocations does not increase and the APT study of section 3.2 confirmed that the concentration of alloy elements in the matrix of the martensite of KNDS4 is not increased during tempering.

Figure 9 furthermore shows that the hardness evolution of the two KNDS4 steels is similar during tempering at 550°C. The hardness decreases by 190 HV during the first 5 minutes of tempering and is thereafter showing an increasing trend. Earlier studies[17] have shown that the hardness decrease of the Fe–C–Mn–Ti steel during the first 5 minutes of tempering at 550°C mainly originate from recovery (approx. 210 HV) and coarsening of Fe_3C (approx. 60 HV).

We use Eq. (2) to calculate the strengthening effect of the cementite precipitates of KNDS4 steel, similar to.[17] The hardness contribution due to small cementite particles in the two KNDS4 steels is 191 HV in the as-quenched state. The hardness decrease due to coarsening of cementite during the first 5 minutes of tempering is thereafter calculated to 98 HV for both KNDS4 steels, since there is no significant difference in the cementite particles of the two KNDS4 steels (Fig. 6). The root cause for the high hardness decrease of KNDS4 steel is that KNDS4 contains a higher volume fraction of small iron carbides in the as-quenched state due to auto-tempering (the auto-tempered regions cover 40–50% of the area in Fe–C–Mn–Ti steel and 80–90% of the area in KNDS4 steel). The coarsening of the iron carbides during early stages of tempering therefore generates a large hardness loss in KNDS4.

The remaining 92.6 HV hardness decrease of KNDS4 steel during the first 5 minutes of tempering (from the total 190 HV measured hardness decrease) is generated by a reduction of the strengthening effect from a combination of solid solution, precipitates and dislocations (recovery). The combined effect of solid solution, precipitates and dislocations is complex. When new precipitates nucleate and grow, they can pin dislocations and reduce recovery. Formation of precipitates will furthermore redistribute alloy atoms from solid solution to the precipitates, which will result in a reduction of solid solution strengthening.

Dislocation strengthening in martensite can contribute to very high levels of hardness in the as quenched state (up to 274 HV),[17] whereas precipitation strengthening gives lower hardness contribution since the precipitates need to grow in size before they generate a hardness contribution. As precipitates nucleate and grow, alloying elements will be redistributed from solid solution to the precipitates. Our APT measurements of the matrix composition of the industrially heat treated KNDS4 steel (Table 3) do however show that the concentration of the alloying elements appear to remain stable in the matrix during tempering. The unaccounted hardness loss of 92.6 HV is therefore expected to be a result of recovery only. Recovery reduces the number of non-indexed points in EBSD whereas carbide nucleation and growth can increase the number of non-indexed points. It is therefore possible that we do not observe any changes in the number of non-indexed points during early stages of tempering of KNDS4.

We conclude that the strength and hardness of KNDS4 can be improved by applying a higher austenitization temperature than the current industrial heat treatment. However, the higher temperature generates a larger grain sizes than the ones resulting from the industrial heat treatment, which can reduce the toughness of the KNDS4 steel[32,33] and is therefore not suitable for engine fasteners. We furthermore conclude that nucleation of complex alloy carbides in martensitic steel that contains several carbide forming elements is more rapid than nucleation of alloy carbides in a steel that contains only one carbide forming element. This observation is supported by literature studies which have shown that nucleation of vanadium and titanium carbides in steel is promoted by Mo additions to the steel.[38–40]

4. Conclusions

We compare the properties of the ultra-high tensile

strength fastener steel KNDS4 and the conventional high strength fasteners steels 34Cr4 and 33B2 at room temperature and at elevated temperatures. We thereafter explain the difference in properties based on a study of the underlying microstructural mechanisms. Finally we perform a heat treatment study of KNDS4 to investigate if the microstructure and properties can be further improved.

KNDS4 steel has a higher yield strength ratio than both conventional high strength steels at 500°C, which have similar yield strength ratios at 500°C. Increased soaking time at elevated temperatures does not influence the yield strength ratio. The nano-indentation creep rate shows a weak trend in which the nano-indentation creep rate is lower as the strength of the different steel grades is higher; KNDS4 (grade 14.9) shows the lowest nano-indentation creep rate, followed by 34Cr4 (grade 12.9) and 33B2 (grade 10.9). The better mechanical properties of the KNDS4 steel are related to alloy carbides in the microstructure. The alloy carbides in KNDS4 are smaller than the alloy carbides in 34Cr4 steel, and the mechanical properties are therefore better. The heat treatment study of the KNDS4 steel shows that changing the standard industrial heat treatment to an austenitization temperature of 1 350°C can increase the hardness of KNDS4 by 8%. The increase stems from a more effective dissolution of alloying elements during the austenitization treatment, which increases the volume fraction of alloy carbides that forms during subsequent tempering and thereby generates precipitation strengthening. However, the standard industrial heat-treatment results in smaller martensite block sizes, which might be more beneficial for the toughness of the steel. Independent of the heat treatment, we find that the mechanical performance of KNDS4 fasteners at elevated temperature and the low nano-indentation creep rates are two strong indicators that fasteners made from KNDS4 steel might be used at higher service temperatures than traditional high strength fasteners.

Acknowledgements

The authors wish to acknowledge the financial support from Koninklijke Nedschroef Holding B. V. CEIC. Ohlund wishes to thank Bosko Pavlovic for support during the analysis of the data.

REFERENCES

1) ISO898-1: 2013, Mechanical properties of fasteners made of carbon steel and alloy steel-Part 1.
2) ASM: ASM Handbook, Failure Analysis and Prevention, Vol. 11, eds. by W. T. Becker and R. J. Shipley, Materials Park, OH, (2002), 818.
3) N. Eliaz, A. Shachar, B. Tal and D. Eliezer: *Eng. Fail. Anal.*, **9** (2002), 176.
4) T. Seguchi, C. Hanai, O. Nakano and Y. Namimura: *JSAE*, 20037061 (2003), 255.
5) Y. Namimura, N. Ibaraki, W. Urushihara and T. Nakayama: *Wire J. Int.*, Jan (2003), 62.
6) S. Freeman and R. W. K. Honeycombe: *Met. Sci.*, Feb (1977), 59.
7) M. Charleux, W. J. Poole, M. Militzer and A. Deschamps: *Metall. Mater. Trans.*, **32A** (2001), 1635.
8) C. Y. Chen, H. W. Yen, F. H. Kao, W. C. Li, C. Y. Huang, J. R. Yang and S. H. Wang: *Mater. Sci. Eng.*, **A499** (2009), 162.
9) S. Shanmugam, M. Tanniru, R. D. K. Misra, D. Panda and S. Jansto: *Mater. Sci. Technol.*, **21** (2005), 883.
10) L. Xu, J. Shi, W. Q. Cao, M. Q. Wang, W. J. Hui and H. Dong: *J. Mater. Sci.*, **46** (2011), 3653.
11) Y. Han, J. Shi, L. Xu, W. Q. Cao and H. Dong: *Mater. Sci. Eng.*, **A530** (2011), 643.
12) R. L. Klueh, N. Hashimoto and P. J. Maziasz: *J. Nucl. Mater.*, **367–370** (2007), 48.
13) K. Maruyama, K. Sawada and J. I. Koike: *ISIJ Int.*, **41** (2001), 641.
14) M. Taneike, N. Fujitsuna and F. Abe: *Mater. Sci. Technol.*, **20** (2004), 1455.
15) P. Michaud, D. Delagnes, P. Lamesle, M. H. Masthon and C. Levaillant: *Acta Mater.*, **55** (2007), 4877.
16) C. E. I. C. Ohlund, J. Weidow, M. Thuvander and S. E. Offerman: *ISIJ Int.*, **54** (2014), 2890.
17) C. E. I. C. Ohlund, D. den Ouden, J. Weidow, M. Thuvander and S. E. Offerman: *ISIJ Int.*, **55** (2015), 883.
18) W. B. Li, J. L. Henshall, R. M. Hopper and K. E. Easterling: *Acta Metall. Mater.*, **39** (1991), 3099.
19) S. Ghodrat: Ph. D. thesis, T. U. Delft, (2013).
20) R. Goodall and T. W. Clyne: *Acta Mater.*, **54** (2006), 5489.
21) C. E. I. C. Ohlund, S. E. Offerman and E. Schlangen: *Mater. Sci. Eng.*, **A560** (2013), 351.
22) L. Zhang, N. Sekido and T. Ohmura: *Mater. Sci. Eng. A*, **611** (2014), 188.
23) M. Thuvander, J. Weidow, J. Angseryd, L. K. Falk, M. Sonestedt, K. Stiller and H. O. Andrén: *Ultramicrosc.*, **111** (2011), 604.
24) B. Huthcinson, J. Hagstrom, O. Karlsson, D. Lindell, M. Tornberg, F. Lindberg and M. Thuvander: *Acta Mater.*, **59** (2011), 5845.
25) L. A. Nordstrom: *Scand. J. Metall.*, **5** (1976), 159.
26) S. Morito, J. Nishikawa and T. Maki: *ISIJ Int.*, **43** (2003), 1475.
27) S. Takebayashi, T. Kunieda, N. Yoshinaga, K. Ushioda and S. Ogata: *ISIJ Int.*, **50** (2010), 875.
28) F-G. Wei, T. Hara, T. Tsuchida and K. Tsuzaki: *ISIJ Int.*, **43** (2003), 539.
29) B. Gault, F. Danoix, K. Hoummada, D. Mangelinck and H. Leitner: *Ultramicrosc.*, **113** (2012), 182.
30) B. Xiao, J. D. Xing, J. Feng, C. T. Zhou, Y. F. Li, X. J. Xie and Y. H. Cheng: *J. Appl. Phys.*, **42** (2009), 5415.
31) T. Gladman: *Mater. Sci. Technol.*, **15** (1999), 30.
32) J. P. Naylor: *Metall. Mater. Trans.*, **10A** (1979), 861.
33) C. Wang, M. Wang, J. Shi, W. Hui and H. Dong: *Scr. Mater.*, **58** (2008), 492.
34) T. Ohmura, K. Tsuzaki and S. Matsuoka: *Philos. Mag.*, **A82** (2002), 1903.
35) S. I. Wright, M. M. Nowell and D. P. Field: *Microsc. Microanal.*, **17** (2011), 316.
36) T. Gladman: The Physical Metallurgy of Microalloyed Steels, The University Press, London, (1997), 33.
37) L. H. Friedman and D. C. Chrzan: *Phys. Rev. Lett.*, **81** (1998), 2715.
38) A. Vyrostakove, A. Kroupa, J. Janovec and M. Svoboda: *Acta Mater.*, **46** (1998), 31.
39) A. Vyrostakove, A. Kroupa, J. Janovec and M. Svoboda: *Acta Mater.*, **46** (1998), 39.
40) J. H. Jang, Y. U. Heo, C. H. Lee, H. K. D. H. Bhadeshia and D. W. Suh: *Mater. Sci. Technol.*, **29** (2013), 309.